Research on Chemical Intermediates (2026) 52:2777–2802
https://doi.org/10.1007/s11164-025-05897-7

Quartz crystal microbalance modified with polyacrylonitrile/polyvinylidene fluoride nanofiber sensor: preparation, characterization, sensor parameters, and adsorption behavior

Rifat Capan[1] · Atike Ince Yardimci[2] · Inci Capan[1] · Yaser Acikbas[3]

Received: 17 October 2025 / Accepted: 20 December 2025 / Published online: 9 January 2026

Abstract

Electrospun nanofibers based on polyacrylonitrile (PAN) and polyvinylidene fluoride (PVDF) have attracted considerable attention owing to their mechanical robustness, thermal stability, and excellent chemical resistance, which make them suitable for use in sensor technologies. In this study, PAN/PVDF nanofibers were produced via electrospinning and characterized by SEM, FT-IR, TGA, and tensile analyses. The SEM images revealed uniform, bead-free, and highly porous nanofibers with an average diameter of 215 ± 29 nm and a porosity of 62.26%. FT-IR spectra confirmed the coexistence and intermolecular interaction of PAN and PVDF phases, while TGA results indicated enhanced thermal stability due to PVDF incorporation. The prepared nanofiber membrane exhibited a Young's modulus of 16.32 MPa and a maximum strain of 42.45%, suggesting high flexibility and strength. The fabricated PAN/PVDF nanofiber film was then integrated into a quartz crystal microbalance (QCM) platform to investigate its vapor sensing behavior against dichloromethane, chloroform, carbon tetrachloride, and trichloroethylene vapors. The ranges of some sensor parameter values, such as sensitivity (0.205–0.249 Hz ppm^{-1}), LOD (160.57–132.53 ppm), and LOQ (487.80–401.60 ppm), are presented for the PAN/PVDF nanofiber-based QCM sensor exposed to these organic vapors. Adsorption dynamics were analyzed using pseudo-first-order and Elovich kinetic models, enabling the evaluation of adsorption parameters and rate constants. The findings demonstrate that PAN/PVDF nanofiber-based QCM sensors offer a promising platform for detecting volatile organic compounds (VOCs), owing to their high surface area, fast response, and stable kinetic performance.

Keywords Polyacrylonitrile · Polyvinylidene fluoride · Nanofiber · Electrospinning · Vapor sensor · Adsorption model

Extended author information available on the last page of the article

Introduction

A wide range of fields have found extensive applications for nanofibers, including high-performance filtration, wound dressing, tissue engineering, vascular grafts, battery separators, energy storage systems, enzyme immobilization, electrochemical sensing, sensor technology, composite reinforcement, and artificial blood vessel engineering. Electrospun nanofibers using natural and synthetic polymers can be easily produced using the electrospinning technique. Polyacrylonitrile (PAN), polyvinylidene fluoride (PVDF), and mixed PAN/PVDF materials prepared as nanofibers are promising candidates for developing chemically and physically stable, sensitive, practical, flexible, and easy-to-use electronic devices. Some examples are given as: the co-electrospun PAN/thermoplastic polyurethane (TPU) nanofiber positive triboelectric layer and PVDF/polydimethylsiloxane (PDMS) nanofiber negative triboelectric layer can be used as self-powered sensors for human movement monitoring and transmitting encrypted information, following Morse code principles [1]. Electrospun graphene oxide-doped PAN, PVDF nanofiber surfaces are used for the development of a flexible piezoelectric vibration sensing element that can be used for detecting dynamic loads on aircraft frames or in developing wearable technologies for pilots [2]. Using the ZnO/PAN and ZnO/PVDF nanofabrics, a mechanically robust pressure sensor and wearable power source, confirmed the potential applications in human activity monitoring and personal thermal management, were studied by Sun [3]. Hydrophobic piezoelectric PVDF-zinc oxide (ZnO) nanofibers are a candidate for this innovative electronic skin, with directional water transport and sensing functions that could ensure long-term wear comfort for practical applications in emerging wearable technologies and all healthcare ranges [4]. Electrospun PAN-derived carbon nanofibers (CNFs) were combined with PVDF nanofibers for piezoelectric nanogenerator applications. It is indicated that harnessing energy from biomechanical movements and ultrasonic wave pressure, thereby exhibiting their applicability in healthcare monitoring devices and sensors [5]. Furthermore, the use of nanofiber materials deposited onto piezoelectric quartz crystal substrates via electrospinning for gas sensor applications has been extensively investigated. This interest stems from their remarkable chemical, mechanical, and physical stability, coupled with a high surface area-to-volume ratio, porosity, and rapid adsorption–desorption characteristics [6]. Recent studies have examined different polyacrylonitrile (PAN)-based quartz crystal microbalance (QCM) nanofiber systems, including pure PAN nanofibers for detecting organic vapors [7], PAN/polypyrrole (PPy) composites [8], PAN/polyvinylidene fluoride (PVDF) hybrid sensors [9], PAN nanofiber blended with citric acid (CA) [10], PAN/chitosan overlaid structures [11], PAN/nickel nanofibers [12], and rhodamine-functionalized PAN nanofibers [13, 14].

The theory of the QCM system is a highly sensitive method for any mass changes deposited onto a quartz crystal substrate. This mass change can be detected on a nanogram scale by measuring a change in the resonance frequency. The frequency change can be monitored as a function of time, which is useful to

monitor molecular interactions or reactions occurring at the electrode surface. As a result of these advantages, the QCM system is preferred for physical, chemical, and biological interactions in gas, VOCs, and biosensor applications. In the QCM technique, the mass change is mainly due to the adsorption and desorption process of vapor molecules on the thin film surface, driven by weak intermolecular forces between the thin film and the vapor molecules [6, 7, 15]. The QCM method is widely used for the adsorption and desorption process of sensor studies because of its high mass change sensitivity on a nanogram scale. In addition, it is portable, easy to operate, low-cost, and allows for the collection of the real-time frequency measurement, which is called the QCM kinetic graph. This graph can be used for sensor parameter and adsorption behavior analysis data collection. Several theoretical models have been developed to analyse adsorption dynamics, including the Pseudo, Elovich, Langmuir, Freundlich, and Langmuir–Freundlich models. These models allow key parameters to be determined, including the adsorption coefficient, adsorption rate, and correlation coefficients [16–18].

The physicochemical interactions between the vapor molecules (analyte) and the thin film (adsorbent) occur, and the pore volume and size distribution of the surface, polarity, molecular weight, saturated vapor pressure of the gas molecules, and external conditions can all play an important role in the adsorption process [19]. Pseudo first-order and Elovich models, known as kinetic models, are commonly used in environmental sciences to describe adsorption behavior. The Pseudo first-order model assumes that the adsorption rate is proportional to the number of available sites, typically describing physisorption limits [20]. The Elovich model describes adsorption on energetically heterogeneous surfaces and is applied to adsorbents on non-uniform solid surfaces, which is useful to reveal data irregularity. Most kinetic models often ignore this irregularity [21]. Adsorption kinetics provide information about the speed of the adsorption process and are one of the main factors that must be understood before the applicability of any adsorbent. The validity of the kinetic models is tested by the correlation coefficient (R^2), which is used as an indicator of the conformity between the model prediction and experimental adsorption data [22].

Studies on VOCs sensor applications of electrospun PAN/PVDF nanofibers are very limited in the literature. The first study of an electrospun PAN/PVDF nanofiber sensor against five different VOCs (chloroform, dichloromethane, trichloroethylene, carbon tetrachloride, and benzene) was reported by our group [9]. It was proven that the PAN/PVDF nanofiber sensor could be a good candidate for a VOC sensor at room temperature. Therefore, this study is focused on an investigation of structural analysis, sensor performance, and adsorption dynamics for the PAN/PVDF nanofiber sensor against chlorinated hydrocarbons. The mechanical robustness, thermal stability, and chemical resistance properties are characterized using Scanning Electron Microscopy (SEM), Fourier Transform Infrared Spectroscopy (FT-IR), Thermogravimetric Analysis (TGA), and tensile analyses. The QCM method is used to monitor the sensor behavior and to collect the experimental data when the PAN/PVDF nanofiber is exposed to vapor molecules.

This work aims to provide a detailed analysis of the obtained results and analyze the adsorption dynamics through the use of Elovich and Pseudo-first-order models. The response and recovery times, humidity influence, reversible

response, long-term stability, selectivity, sensitivity, limit of detection (LOD), and the limit of quantification (LOQ) parameters of the PAN/PVDF nanofiber sensor are determined using SPR kinetic measurement. In addition, the adsorption behavior is studied using Pseudo-first-order and Elovich models to calculate the equilibrium density (q_e), the first-order rate constant, and the correlation coefficient values.

Material and methods

Sample preparation and characterization

To produce the PAN/PVDF electrospun nanofibers, PAN (MW = 150.000, CAS No.: 25014-41-9), PVDF (MW ~ 180.000, Mn ~ 71.000, in pellet form, CAS No.: 24937-79-9), and N,N-dimethylformamide (DMF, anhydrous, 99.8%, CAS No.: 68-12-2) were sourced from Sigma-Aldrich. In our previous studies, PAN:PVDF ratios of 95:5, 90:10, 85:15, 80:20, and 75:25 were tested for nanofiber production. SEM images showed that the average diameter of electrospun PAN/PVDF nanofibers containing 20 wt% PVDF was lower than that of other nanofibers. Nanofiber morphology, microstructure, and diameter directly affect the sensing performance of gas sensors, with lower diameters providing advantages in sensor performance [9, 23]; therefore, 20 wt% PVDF was used in this study.

A dimethylformamide (DMF) solution with a total polymer content of 8 wt%, consisting of 20% polyvinylidene fluoride (PVDF) and 80% polyacrylonitrile (PAN), was homogeneously obtained by stirring at 60 °C for a total of 4 h. The resulting solution was filled into a 5 ml syringe, and fiber production was carried out by electrospinning at a voltage of 15 kV with a flow rate of 1.5 µL/h for 4 h. The resulting PAN/PVDF fibers were collected on a collector coated with Al foil and a QCM placed on it. The electrospinning coating of PAN/PVDF nanofibers on the QCM is shown in Fig. 1.

Scanning electron microscopy (SEM, Zeiss–Model LEO 1430 VP) was used to characterize the surface structure of PAN/PVDF nanofibers. Before imaging, the samples were coated with a thin layer of gold and examined using the secondary electron mode. Analysis was performed at 20 kV.

Diameter measurements were taken from the SEM image to determine the diameter distribution of the PAN/PVDF nanofibrous sample. The diameters of 52 fibers were measured, and then the average fiber diameter was calculated.

The porosity value of the first layer of the nanofiber film was calculated using SEM imaging in MATLAB. The porosity ratios of PAN/PVDF nanofibers were calculated from the pixel value for each location in the binary black-and-white image after segmentation. The porosity value was calculated by dividing the number of white pixels in the SEM image by the total number of pixels [24]. Three SEM images taken from different areas of the PAN/PVDF nanofibrous sample at 25,000X magnification were used to calculate the porosity value.

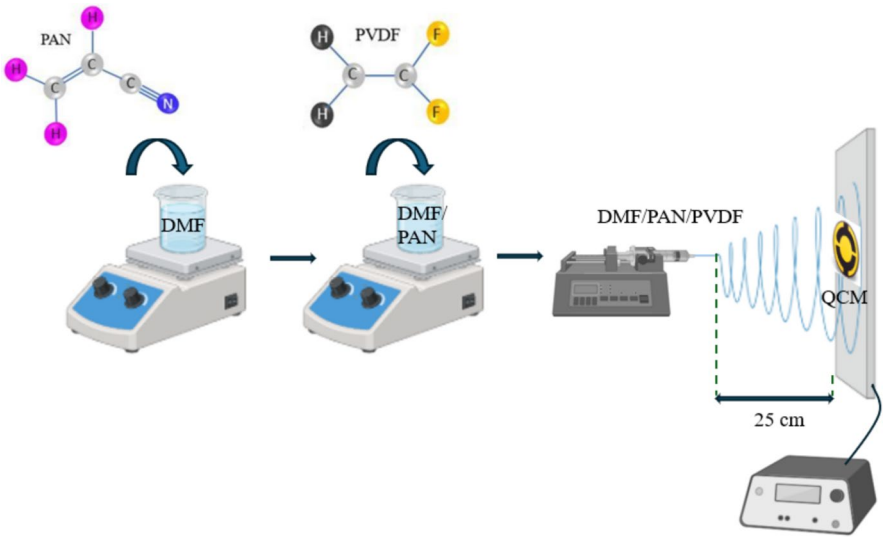

Fig. 1 Schematic representation of PAN/PVDF nanofiber coating on QCM by electrospinning method

$$p\,(\%) = \left(\frac{n}{N}\right)100$$

Structural characterization was performed using Fourier Transform Infrared Spectroscopy (FT-IR, Spectrum Two UATR-FTIR, Perkin Elmer Corp., Norwalk, CT, USA) in the scanning range of 4000–450 cm^{-1}. Thermogravimetric analysis (TGA, Shimadzu TGA-51) was used to evaluate the thermal properties of the fibers. TGA analysis was performed by heating at a rate of 10 °C/min in a N_2 atmosphere between 25 and 800 °C.

A tensile test was performed to determine the mechanical properties of PAN/PVDF nanofibers. To prepare the test sample, pieces measuring 60 mm × 8 mm were cut from the nanofiber membrane. A 5 kg load cell was used for the tensile tests. The device used was a TA.XT Plus (Stable Micro Systems Ltd., Surrey, England) texture analyzer, and the test was performed at a rate of 1 mm/min.

QCM measurement system

The QCM measurement technique is based on assessing the resonance frequency of a piezoelectric quartz crystal, achieved by applying an appropriate voltage through gold electrodes. The electrospun PAN/PVDF nanofiber-based QCM sensor is deposited onto an AT-cut quartz crystal with a frequency of 8 MHz, commercialized by the company GTE SYLVANIA. It is sandwiched between metal electrodes on both sides. Figure 2 shows a schematic representation of a homemade QCM system that is fully computer-controlled.

The PAN/PVDF nanofiber-based QCM sensor is connected to an oscillator circuit, allowing the quartz crystal to oscillate at its resonance frequency via an

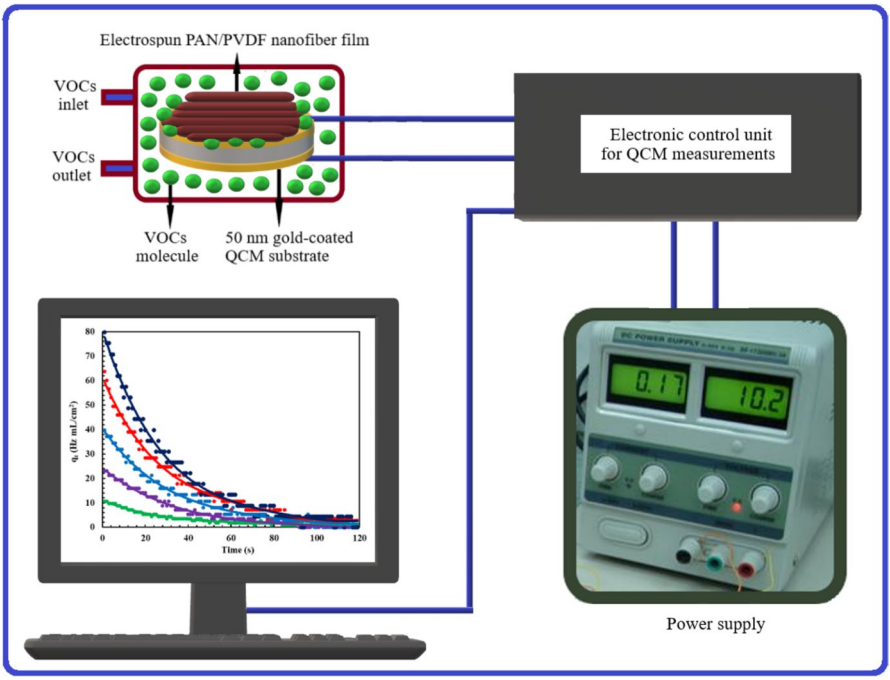

Fig. 2 A representation of a homemade QCM system

alternating voltage applied by a DC power supply on the electrodes. Additionally, an electronic control unit is used to detect any frequency changes of the PAN/PVDF nanofiber-based QCM sensor by the QCM oscillator. All data was collected with a PC with specialized software. If vapor molecules interact with QCM sensors, the frequency should be changed proportionally with vapor mass deposition. The relation between frequency change (f) and deposited mass (m) was discovered by Sauerbrey [25] given as:

$$\Delta f = -\left(\frac{2f_0^2}{\rho_q^{1/2}\mu_q^{1/2}A}\right)\Delta m \tag{1}$$

where f_0 is the initial frequency of uncoated quartz crystal (7,983,236 Hz), A is the piezo-electrically active area (0.196 cm^2), $_q$ is the density of quartz (2.648 g cm^{-3}), $_q$ is the shear modulus of quartz (2.947×10^{11} g cm^{-1} s^{-2}).

The Sauerbrey equation is valid under the assumption that the added mass forms a thin, rigid, and homogeneous film, and that the associated frequency shift (Δf) is small compared to the crystal's fundamental resonance frequency (f). This requirement is generally expressed as $\Delta f/f < 0.05$ [26], ensuring that the perturbation caused by the mass loading does not alter the cut-off oscillation mode or result in significant viscoelastic effects. Considering this information, the observed frequency shifts in our measurements are only a few hundred hertz.

For an 8 MHz AT-cut quartz crystal, such shifts correspond to a relative change of the order of 10^{-5}–10^{-4}, which is several orders of magnitude below the 0.05 threshold. Consequently, the system operates well in the linear regime, and all the conditions necessary for correctly applying the Sauerbrey relation are satisfied.

To study the vapor interaction with the PAN/PVDF nanofiber-based QCM sensor, an isolated gas cell with inlet and outlet holes is used. Each organic vapor was taken using a Hamilton syringe and injected into the gas cell, allowing for 2 min to interact with the PAN/PVDF nanofiber-based QCM sensor, followed by another 2 min in which dry air was injected. The final data is recorded in the form of frequency change over time, known as the real-time QCM kinetic response, which is valuable for determining the sensor parameters and characteristics of the PAN/PVDF nanofiber-based QCM sensor. The increasing saturated vapor concentration ratios of 20%, 40%, 60%, 80%, and 100% were distinguished to study the concentration effect between the PAN/PVDF nanofiber-based QCM sensor and selected vapor. In three kinetic cycles, 100% of the saturated concentration value was applied onto the PAN/PVDF nanofiber-based QCM sensor for the stability and reproducibility test. All data were recorded at room temperature (20 °C) with a resolution of 1 Hz.

Adsorption theory and fitting models

Studies on gas sensors have focused on the synthesis of new materials and the preparation of highly sensitive sensor elements. Nanofibers have found a wide range of applications across several industries and fields, such as sensors for environmental remediation, biomedical and healthcare, tissue engineering, and drug delivery systems. [27, 28]. They are suitable for the field of air and water filtration, adsorption of pollutants, and removal of contaminants. Recently, nanofibers have been utilized as sensitive sensor elements for gas or vapor sensor applications due to their high adsorption capacity, fast response and recovery times, ease of fabrication, low cost, and stability [29, 30]. Investigating the adsorption dynamics between gas or organic vapor molecules interacting with the nanofiber sensor material is crucial for elucidating the sensor interaction mechanism. Elucidating these interaction mechanisms contributes to the design of new synthesized substances. Adsorption dynamics play a significant role in the interactions between nanofiber sensors and the adsorbate. To study adsorption dynamics, several fitting models such as the Elovich, Pseudo-first-order, Pseudo-second-order, Ritchie, Scatchard, Langmuir, Freundlich, and Langmuir–Freundlich models have been developed for analyzing experimental data taken by QCM, SPR, electrical, and optical measurement systems during the interaction between the sensor element and gas/vapor molecules [15, 18, 31].

To analyze the adsorption dynamics, the adsorption capacity, or the adsorption amount per unit area, q_t, of a QCM nanofiber sensor should be calculated using the real-time experimental data collected during the interaction of the sensor material with vapor molecules. q_t is described in Eq. 2 [14].

$$q_t = \left[\frac{(q_i - q_e)V}{A}\right] \tag{2}$$

where q_i and q_e are the initial frequency and the equilibrium frequency, respectively. A is the nanofiber sensor surface area, V is the injected vapor volume, respectively.

The Lagergren's Pseudo first-order kinetic equation is given by [13]:

$$\frac{dq_t}{dt} = k_1(q_e - q_t) \tag{3}$$

where k_1 is the Pseudo first-order adsorption rate constant. q_e is the amount of vapor molecules at equilibrium and q_t is the amount of vapor molecules adsorbed at time t, respectively.

Equation 3 is rearranged as:

$$\frac{dq_t}{(q_e - q_t)} = k_1 dt \tag{4}$$

Using boundary conditions, it is integrated and can be arranged as:

$$\log\left(\frac{q_e}{q_e - q_t}\right) = \frac{k_1}{2.303}t \tag{5}$$

Finally, Eq. 5 can be given in a linear form:

$$\log(q_e - q_t) = \log q_e - \frac{k_1}{2.303}t \tag{6}$$

A frequency change happens if vapor molecules interact with a sensitive sensor element. This change depends on the amount of adsorbed vapor molecules (q_t). A plot of log (q_e – q_t) as a function of t gives a linear relationship. The Pseudo first-order model allows us to analyze the adsorption process using the slope $\left(\frac{k_1}{2.303}\right)$ and the intercept $(\log q_e)$. Using Eq. 6 and QCM experimental data for the (PAN/PVDF) nanofiber-based QCM sensor, k_1, q_e can be determined. The correlation coefficient (R^2) for the graph of log (q_e–q_t) versus t is an important indicator for the conformity of fitting parameters.

The Elovich model is another adsorption process analyzing model using QCM experimental data. The adsorption rate (dq_t/dt) in the Elovich model is given as:

$$\frac{dq_t}{dt} = a\exp(-bq_t) \tag{7}$$

where a is the initial adsorption rate, b is the Elovich desorption constant and q_t is the quantity of adsorbed gas at time t, respectively. If q_t is chosen 0, Eq. 7 is equal to a. If the boundary conditions are chosen from $q_t = 0$ at t=0 to $q_t = q_t$ at t=t, Eq. 7 can be easily integrated as:

$$q_t = \left(\frac{1}{b}\right)\ln(ab) + \left(\frac{1}{b}\right)\ln t \tag{8}$$

If it is assumed that $t \gg t_0$, a plot of q_t versus *lnt* gives a linear relationship. It can be used to determine the a, b constants, and the correlation coefficient (R^2) values. Using Eq. 8 and QCM experimental data, these parameters of the PAN/PVDF nanofiber-based QCM sensor are calculated in this study.

Gas sensing measurements for sensor parameters

The gas sensing properties of the PAN/PVDF nanofiber-based QCM sensor were investigated using the QCM technique. Chlorinated vapors: chloroform, dichloromethane, carbon tetrachloride, and trichloroethylene, with their five different concentration values, were injected into the gas cell with a time interval of 120 s. Within each reciprocal 120 s, increasing amounts of saturated vapor were injected into the gas cell. 120 s of dry air injection was introduced into the gas cell for recovery between each vapor injection. The sensor response measurements were taken 3 times.

The frequency change (Df) as a function of concentration (c) was modelled via a linear dependence and the sensitivity (S) values, which are defined as:

$$S = \mathrm{Df} / c \tag{9}$$

was obtained by the slope of this linear dependence.

The limit of detection (LOD) and the limit of quantification (LOQ) values were calculated accordingly using Eqs. 10 and 11, where σ is the standard deviation of the QCM instrument ($\sigma = 1$ Hz).

$$\mathrm{LOD} = 3.3\sigma / \mathrm{S} \tag{10}$$

$$\mathrm{LOQ} = 10\,\sigma / \mathrm{S} \tag{11}$$

In order to investigate the PAN/PVDF nanofiber-based QCM sensor performance, such as humidity effect, long-term stability, reversibility, and selectivity, DCM vapor was chosen because of the highest sensitivity value of DCM vapor. To test the long-term stability of the sensor, the kinetic vapor sensing measurements using DCM vapor were recorded during the initial thin film fabrication (A) and the thin film after 2 years (B). Another experiment was carried out on the interactions reversible over many cycles. All experimental results and calculated data are given in "Sensor performance parameters" section.

Results and discussion

Morphological and structural properties of the PAN/PVDF nanofibers

Before determining sensor properties, it is crucial to observe whether the PAN/PVDF nanofibers form a complete film structure. Therefore, the morphologies of the

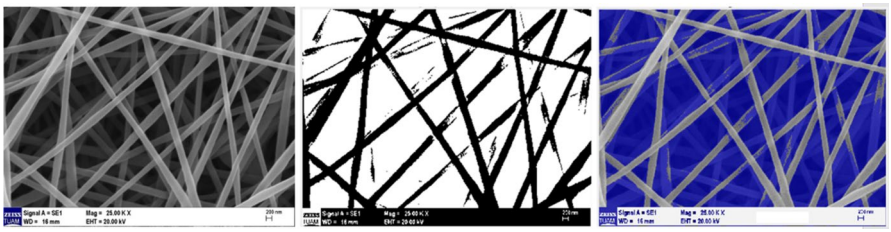

Fig. 3 **a** Original SEM image of PAN/PVDF nanofibers, **b** binary (fiber and pore), **c** porosity of PAN/PVDF nanofiber obtained from Matlab program

PAN/PVDF nanofibers were examined using SEM, and the SEM image is presented in Fig. 3a. SEM images reveal that the nanofibers are capable of forming a complete film structure, and the fiber structure is quite regular and homogeneous. When examined individually, the fibers are also observed to be bead-free and smooth.

2D porosity obtained through MATLAB-based SEM image analysis is a common and accepted approach, but this value generally represents the areal porosity of selected images, not the 3D porosity of the entire membrane [32, 33]. Therefore, to reduce the margin of error, three SEM images taken from different areas of the PAN/PVDF nanofibrous sample were analyzed and averaged using MATLAB. The porosity value of the first layer of the nanofiber film is $76.51 \pm 16\%$. The images of the first layer, whose porosity was examined, are shown in Fig. 3b, c. The suitability of this porosity value in the first layer for gas sensor applications was evaluated in the sensor portion of the study.

The average diameter of PAN/PVDF nanofibers was determined as 231.37 ± 40.73 nm. The diameter distribution graph showed fiber formation in the diameter range of 160–360 nm. The diameter distribution graph is depicted in Fig. 4.

The FT-IR graph of PAN/PVDF nanofibers, whose structural properties were investigated by FT-IR spectroscopy, is plotted in Fig. 5. In the FT-IR spectrum, the characteristic bands of PAN were observed at 1454 and 2240 cm^{-1}, and these peaks correspond to the C=C and –C≡N stretching vibrations, respectively [34]. In the sample containing PVDF, the peaks at 1405 and 1198 cm^{-1} represented the symmetric stretching vibrations of $–CF_2$ groups, and these bands confirmed the presence of these bands in the electrospun fibers as characteristic signs of PVDF. In addition, the C–F stretching vibration of the amorphous phase was determined by the FT-IR signals at 885 cm^{-1}.

In the FT-IR spectrum of PVDF, strong absorptions observed in the 763–795 cm^{-1} band indicate the presence of the α-phase. The peak around 840–842 cm^{-1} originates from the β-phase. A broad peak in the 825–835 cm^{-1} range indicates a γ-phase contribution. Furthermore, the broad absorption observed in the 1230–1280 cm^{-1} range suggests that the β (1275 cm^{-1}) and γ (1234 cm^{-1}) peaks overlap [35]. In the FT-IR spectrum of the PAN/PVDF sample, the phase peaks of PVDF are still detectable. The α-phase peak is present around 763 cm^{-1}, and the β-phase peak around 840–842 cm^{-1} has decreased in intensity but not disappeared. Mixing with PAN did not destroy the crystalline phases of PVDF, but rather reduced their intensity. The

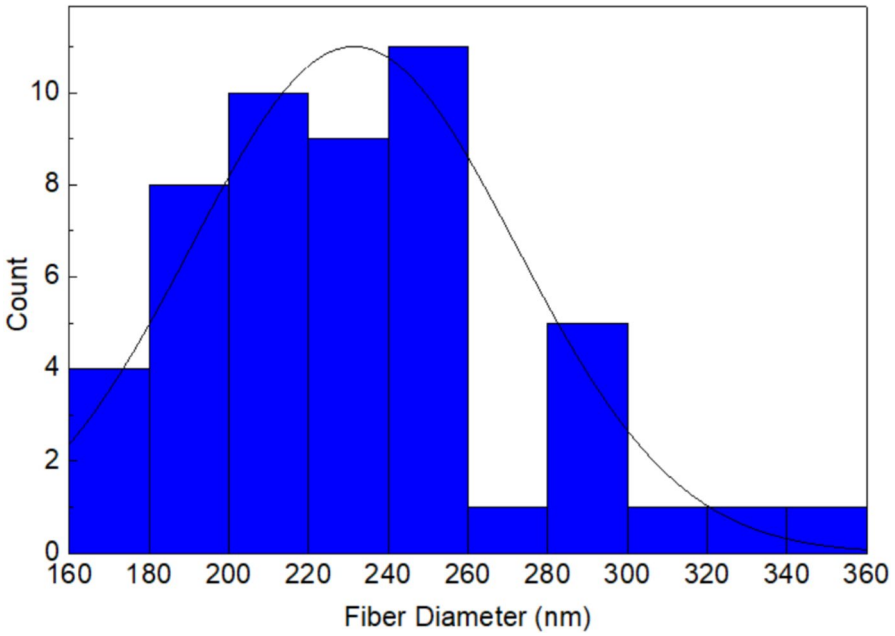

Fig. 4 Diameter distribution of PAN/PVDF nanofibers

C≡N peak of PAN is clearly visible in the PAN/PVDF composite nanofibers at a wavenumber of 2240 cm^{-1}. FT-IR results indicate that PAN and PVDF do not react chemically, but are merely a physical mixture.

Thermal and mechanical properties of the PAN/PVDF nanofibers

The thermal properties of PAN/PVDF nanofibers were investigated using a TGA device. When the TGA graph was examined, it was seen that thermal decomposition occurred at two different points after the water vapor in the PAN/PVDF sample evaporated up to 100 °C. The first decomposition occurred around 370 °C, as seen in Fig. 6. The decomposition temperature of PAN is known to be in the range of 210–410 °C [23]. Therefore, it is observed that the decomposition that occurred at this temperature was due to PAN. The second decomposition occurred around 670 °C. This decomposition was due to PVDF [36]. The addition of PVDF to PAN improved the thermal properties of the nanofibers. In the TGA graph, almost no residue was observed after the combustion decomposition of the PAN/PVDF polymers.

PVDF is a semi-crystalline polymer characterized by high tensile strength and impact resistance. These properties are closely related to the strong C–F bonds in its chain structure and the crystalline phase ratio. Furthermore, as the β-phase abundance of PVDF increases, its flexibility and piezoelectric performance, as well as its mechanical strength, improve significantly [37]. Using PAN and PVDF together, a nanomaterial with excellent mechanical properties was obtained. To examine the

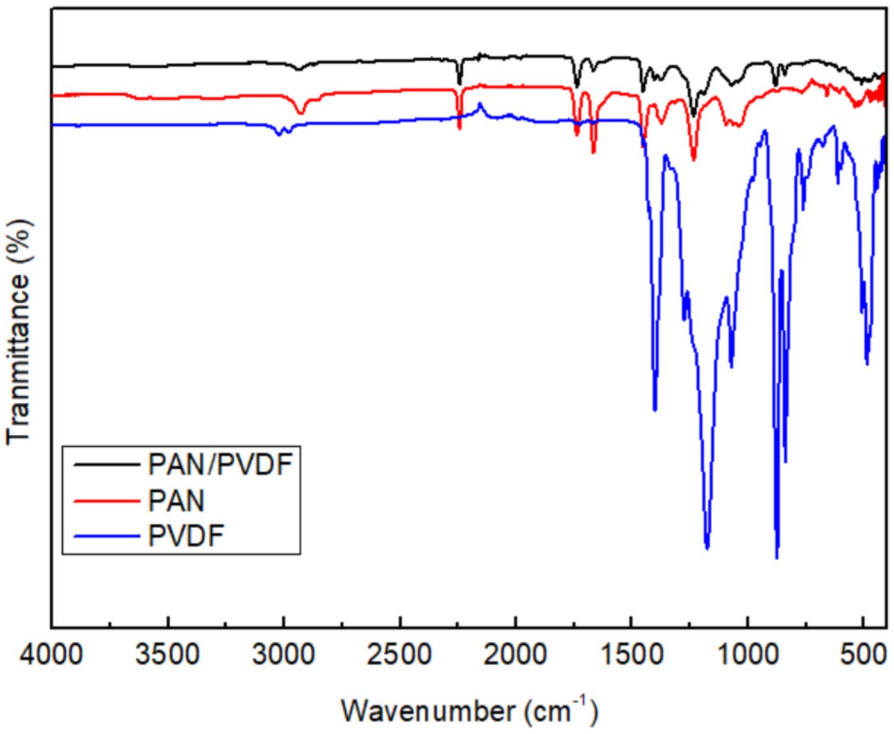

Fig. 5 FT-IR spectra of PAN, PVDF, and PAN/PVDF nanofibers

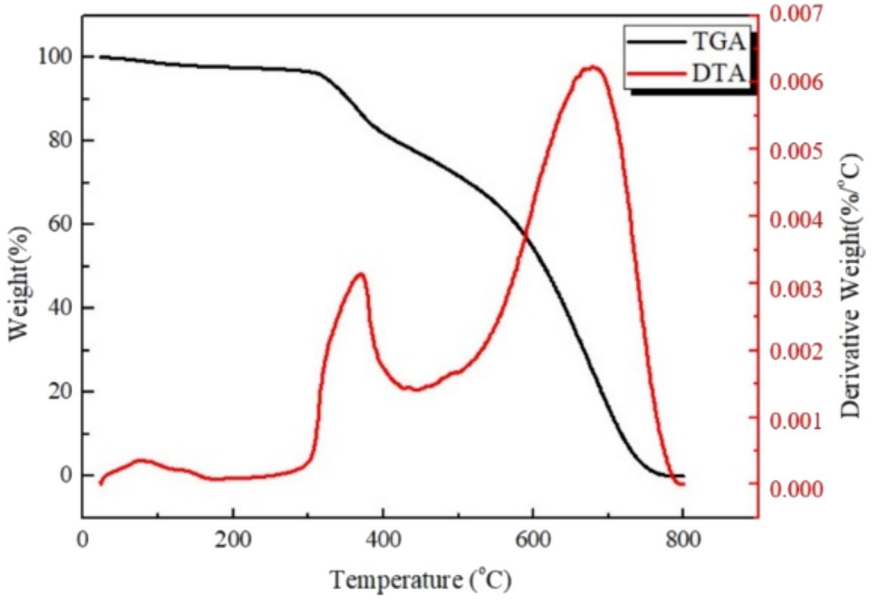

Fig. 6 TGA–DTA graph of PAN/PVDF nanofibers

mechanical properties, a tensile test was performed on the nanofiber membrane. The membrane used in the test was approximately 400 µm thick. The force-percentage elongation graph summarizing the material's mechanical properties is presented in Fig. 7. The Young's modulus of the nanofibers is 16.32 MPa, the maximum strain value is 42.45%, and maximum stress was found to be 2.11 MPa. When the tensile test graph in Fig. 7 is examined, it is observed that the graph appears noisy due to the nanofibers breaking individually after a certain extension under force. The fact that not all fibers break suddenly supports the flexible structure. Unlike our study, Elkhaldi and colleagues [38] obtained PAN/PVDF nanofibers by impregnating PAN nanofibers with PVDF particles in solution. Supporting PAN nanofibers with PVDF particles improved Young's modulus and tensile strength [39–41]. Therefore, the literature also supports the notion that PVDF improves the mechanical properties of PAN nanofibers.

Gas sensing measurements and sensor parameters

The kinetic graph of chloroform vapor is presented in Fig. 8. The kinetic graphs of dichloromethane, trichloroethylene, and carbon tetrachloride vapors are given in the Supplementary Materials (Figs. S1–S3). The presented sensor response data in this section are based on previously published experiments [9].

Each concentration was prepared via a syringe of volume 5 mL. 20% of saturated vapor volume (1 mL) was mixed with dry air in the syringe and injected into the

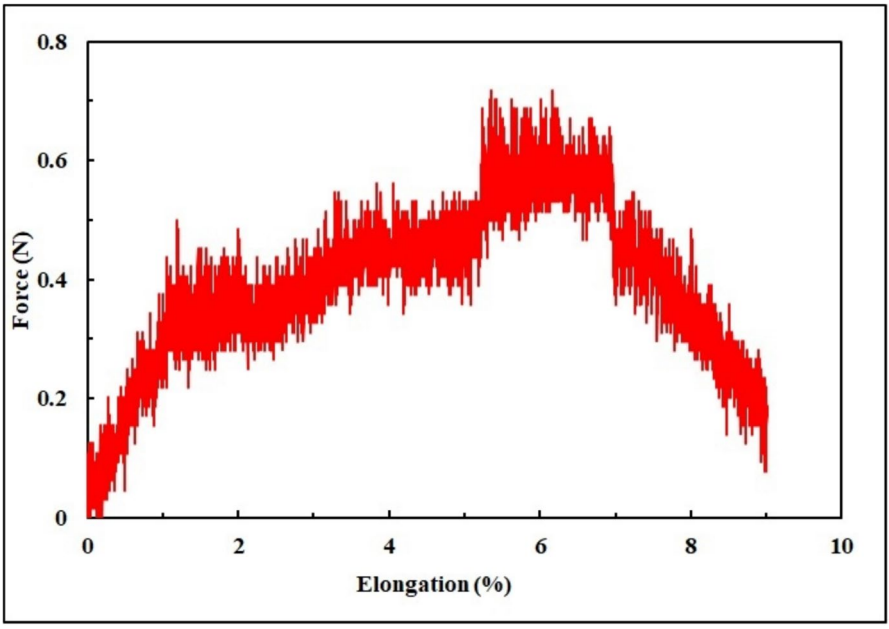

Fig. 7 Force–Elongation graph of PAN/PVDF nanofibers

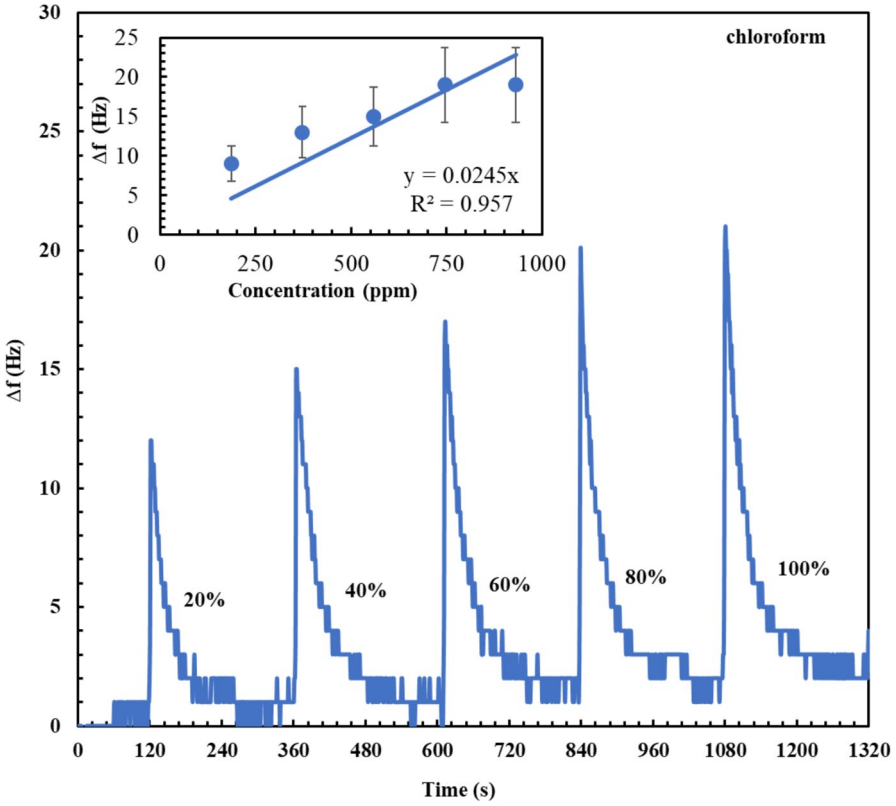

Fig. 8 PAN/PVDF nanofiber sensor response to chloroform vapor at different concentrations. Inset: calibration graph to increasing concentrations

gas cell for the first cycle of the kinetic measurement. The increasing vapor content was used for the reciprocal cycles to obtain from 20 to 100% saturated vapor using the same injector. 120 s were allowed for each interaction between the PAN/PVDF nanofiber-based QCM sensor and chlorinated vapors. Between each interaction, dry air was injected into the gas cell by a clean 5 mL injector for recovery. The kinetic graphs of the PAN/PVDF nanofiber-based QCM sensor are exposed to increased concentrations of chloroform vapor up to the saturated vapor value. The inset in each figure presents the frequency shift due to the injected vapor amount, which is given in terms of vapor concentration in ppm. All sensitivity values calculated using Eq. 9 and the inset graph in Fig. 8 were listed in Table 1 for each chlorinated vapor tested. The regression coefficients were close to unity and acceptable. The LOD and LOQ values of the PAN/PVDF nanofiber sensor are calculated using Eqs. 10 and 11 given in Table 1. The highest sensitivity value was obtained for dichloromethane vapor, and hence the lowest LOD and LOQ values among all chlorinated vapors tested.

In the sensor applications, VOCs' properties given in Table 2 are playing an important role.

Table 1 Sensor parameters of PAN/PVDF nanofiber sensor

VOC	Response time (s)	Recovery time (s)	Sensitivity (Hz ppm^{-1})	LOD (ppm)	LOQ (ppm)	Regression coefficient (R^2)
Dichloromethane	3	6	0.0249	132.53	401.60	0.9899
Chloroform	4	8	0.0245	134.69	408.16	0.9570
Carbon tetrachloride	5	11	0.0234	141.02	427.35	0.9845
Trichloroethylene	5	12	0.0205	160.97	487.80	0.9842

Table 2 The physical properties of VOCs

VOC	Molar mass (g mol^{-1})	Vapor pressure (kPa)	Dipole moment (D)
Dichloromethane	84.93	57.3	1.60
Chloroform	119.37	25.9	1.15
Carbon tetrachloride	153.81	11.94	0
Trichloroethylene	131.38	7.8	0.77

Of the vapors examined, the PAN/PVDF nanofiber sensor demonstrated the highest sensitivity towards dichloromethane vapor. It has the lowest molar mass, which can be explained by the fact that it can easily penetrate the PAN/PVDF nanofiber sensor structure [42]. The dichloromethane vapor pressure is much higher than that of other vapors, which could yield a surface interaction between the vapor molecules and the nanofiber sensor, contributing to a higher frequency shift [43]. Because of its relatively high dipole moment, dichloromethane vapor exhibits stronger electrostatic interactions with the polar surfaces of the PAN/PVDF nanofiber sensor, which in turn enhances electron transfer processes [44]. All these interactions are attributed to the adsorption processes [45, 46].

While studies focusing on PAN/PVDF nanofiber sensors fabricated by electrospinning for the detection of chlorinated hydrocarbon vapors are limited, there have been several investigations into QCM-based vapor sensors reported in the literature. A comparative overview of these studies is provided in Table 3.

Concentration dependence parameters of adsorption dynamics

The Elovich and Pseudo first-order model parameters are both calculated via Eqs. 2, 6, 8, and Figs. 9, 10 and 11. Table 4 gives the calculated fitting parameters of two adsorption models. According to the Pseudo first-order model, k_1 and q_e values were observed to increase as the chloroform vapor concentration increased. In the Elovich model, the *a* value increased as the chloroform concentration increased, while the *b* value decreased. In terms of R^2 values, the Elovich model showed a higher fit than the Pseudo first-order model. This indicated that chloroform vapor interacted with the sensor material, and the Elovich adsorption model is more suitable than the Pseudo first-order model.

Table 3 The sensitivity, LOD, and LOQ values of the PAN derivative QCM nanofiber-based sensors in the literature

Nanofiber-based QCM sensor	VOC	Sensitivity	LOD	LOQ	References
PAN	Chloroform Carbon tetrachloride	0.0217 Hz/ppm 0.0158 Hz/ppm	152.07 ppm 208.86 ppm	460.81 ppm 632.90 ppm	[15]
PAN-RHE	Chloroform Thrichloroethylene Carbon tetrachloride	0.0276 Hz/ppm 0.0151 Hz/ppm 0.0201 Hz/ppm	119.56 ppm 218.54 ppm 164.17 ppm	362.31 ppm 662.25 ppm 497.51 ppm	[15]
PAN/Ni	Methanol	389.8 ± 3.8 Hz/SCCM	1.347 SCCM (range of concentration between 7 and 550 ppm)	not reported	[47]
PAN PAN/CA	Ammonia	0.075 Hz/ppm 0.28 Hz/ppm	not reported not reported	not reported not reported	[10]
PAN	Safrole	4.6 Hz L/mg	not reported	not reported	[48]
PAN-RHE	Dichloromethane	0.0215 Hz/ppm	153 ppm	465 ppm	[13]
PAN-RHE	Acetone Ethanol	0.0243 Hz/ppm 0.0091 Hz/ppm	135.80 ppm 362.63 ppm	411.52 ppm 1098.9 ppm	[14]
PAN/PVDF	Dichloromethane	0.0249 Hz/ppm	132.53 ppm	401.60 ppm	[9]
PAN/PVDF	Chloroform Carbon tetrachloride Thrichloroethylene	0.0245 Hz/ppm 0.0234 Hz/ppm 0.0205 Hz/ppm	134.69 ppm 141.02 ppm 160.97 ppm	408.16 ppm 427.35 ppm 487.80 ppm	This study

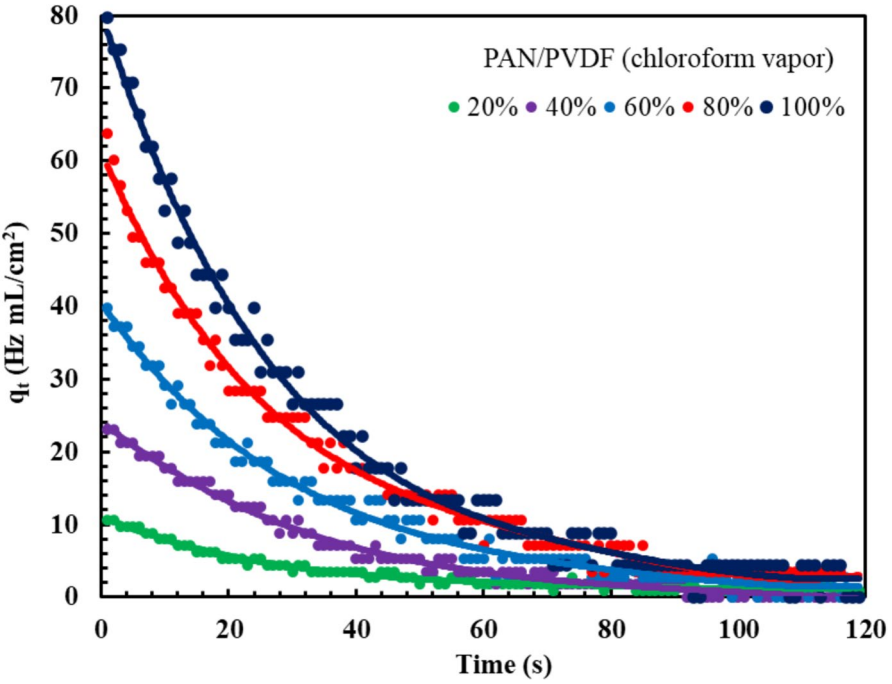

Fig. 9 q_t versus time for chloroform vapor

Similar calculations are followed for other (dichloromethane, trichloroethylene, and carbon tetrachloride) vapors and are reported in the Supplementary Materials (Figs. S4–S12 and Tables S1–S3). All results show a similar trend to chloroform vapor. If we take notice of the R^2 values for each concentration value, the R^2 value of the Elovich model is always higher than the values of the Pseudo first-order model. It can be concluded that our experimental results can be explained by the Elovich model.

The Elovich model results could be summarized as the adsorption features of the PAN sensor have a non-uniform solid surface. Different types of QCM-based PAN nanofiber sensors given in Table 3 were studied for VOC sensor applications. The interaction of the vapor molecules with the nanofiber sensor PAN is believed to start with a condensation on the surface of the nanofiber sensor, followed by an adsorption process. The sensing mechanism of the vapor molecules with the nanofiber sensor structure is affected by the ability of the vapor molecules to be held up on the surface as a result of the intermolecular forces, such as hydrogen bonding, dipole–dipole interaction, and Van der Waals bonding [13, 49, 50]. All these effects are directly related to physical properties such as vapor pressure, molar mass, dipole moment, given in Table 2, and the chemical structure of the vapor molecules [7, 15]. Several mechanisms have been reported in the literature for the adsorption process, including hydrogen bonding, dipole–dipole, ion–dipole, n-π, and π-π interaction [7–9, 51].

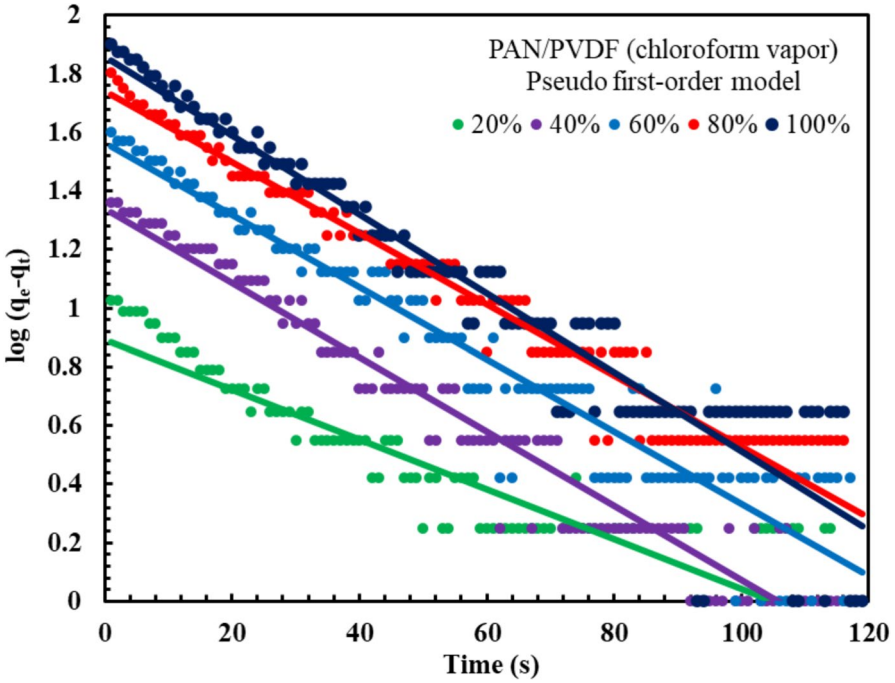

Fig. 10 The fitting performance of the pseudo-first-order model

100% response parameters of adsorption dynamics

For the reproducibility test of the PAN/PVDF nanofiber-based QCM sensor, three cycles of exposure using the saturated vapors were executed. The kinetic graphs of each vapor were presented in Fig. 12. The responses in frequency shift showed similar values for reciprocal exposures.

Adsorption coefficients were calculated using the Elovich model for the 3-cycle results, with a 100% concentration value applied to all vapors. Average values and standard deviations were obtained and shown in Table 5. The highest value of a was obtained for chloroform vapor, while the lowest value of a was obtained for trichloroethylene vapor.

Sensor performance parameters

The PAN/PVDF nanofiber-based QCM sensor was exposed to 2 mL of air with 88% RH; air with 88% RH mixed with saturated dichloromethane vapor, 1 mL in volume each; 2 mL of saturated dichloromethane vapor. A 120 s time interval allowed for the sensor to interact with the vapors. The result is presented in Fig. 13. If the water molecules in this injection have an effect on the gas sensing performance, a more

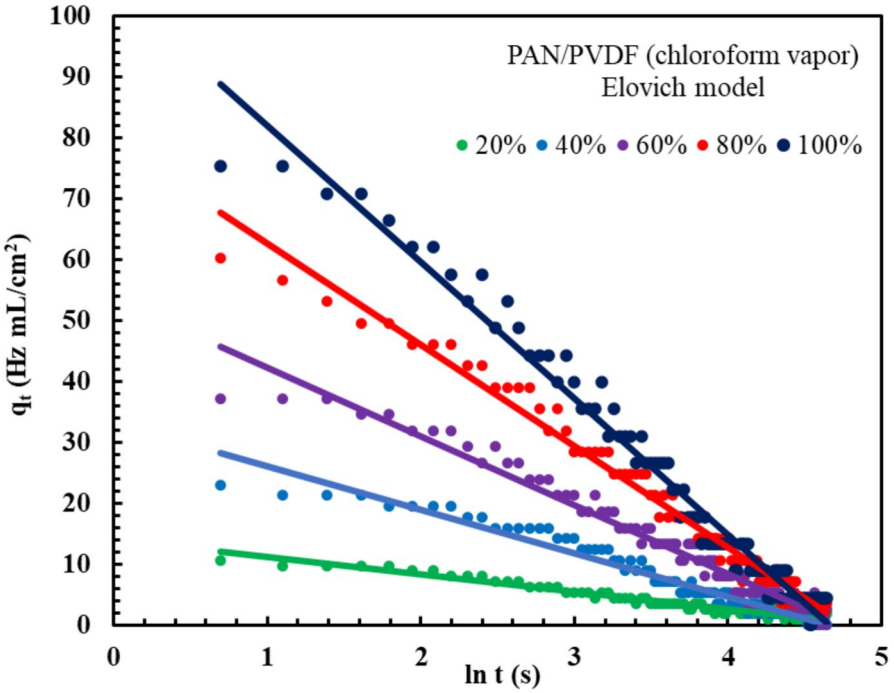

Fig. 11 The fitting performance of the Elovich model

Table 4 Model fitting results for the PAN/PVDF nanofiber-based sensor QCM sensor

Chloroform Concentration (%)	Pseudo-first order model			Elovich Model		
	k_1 (Hz mL/cm^2)	q_e (cm^2 s /Hz mL)	R^2	a (Hz mL/cm^2)	b (cm^2 s /Hz mL)	R^2
20	0.0195	7.8036	0.840	381.3214	0.3518	0.963
40	0.0290	21.8122	0.956	751.6549	0.1404	0.961
60	0.0283	36.7451	0.921	1298.8712	0.0885	0.969
80	0.0278	55.3095	0.952	1955.8549	0.0602	0.983
100	0.0310	72.5938	0.901	2371.6066	0.0447	0.976

significant response would accompany the injections containing an 88% RH value. Therefore, the effect of relative humidity in air was found to be negligible according to Fig. 13.

Figure 14 presents the long-term stability of the PAN/PVDF nanofiber-based QCM sensor after 2 years. The same procedure was followed for the measurements recorded 2 years after the initial measurement; increasing saturated concentrations (20%–40%–60%–80%–100%) of the dichloromethane vapor were exposed in 5 cycles, where 2 min of interaction time was allowed within each

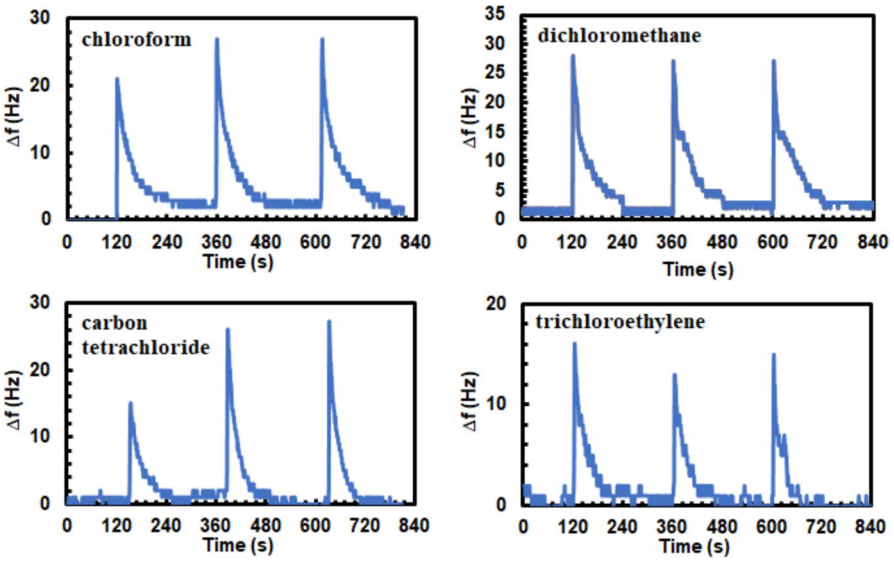

Fig. 12 Three cycles at 100% concentrations of the PAN/PVDF nanofiber-based QCM sensor

Table 5 Adsorption coefficients of the PAN/PVDF nanofiber-based QCM sensor

Vapor	$\overline{a} \pm \sigma$	$\overline{b} \pm \sigma$	$\overline{R^2}$
Dichloromethane	2641.16 ±174.81	0.0392 ±0.003	0.954
Chloroform	3110.97 ±650.51	0.0416 ±0.003	0.982
Carbon tetrachloride	2285.58 ±215.94	0.0372 ±0.007	0.977
Trichloroethylene	1747.19 ±375.82	0.0661 ±0.008	0.937

cycle and a flushing with air period. A response loss of approximately 25%, %, 23%, 29%, 9%, 15% was calculated for each reciprocal cycle of exposures for 20%, %, 40%, 60%, 80% and 100% of saturated dichloromethane vapor.

Another experiment was carried out on the interactions reversible over many cycles. The response of the PAN/PVDF nanofiber-based QCM sensor over 25 reciprocal cycles is presented in Fig. 15. 2 min of interaction time period was allowed for the sensor during each exposure to the saturated concentration of dichloromethane vapor, and 1 min of time was allowed for the sensor to recover. The reversible interaction over 25 cycles was observed, and it can be concluded that the sensor can be used at least for 25 cycles.

To investigate the sensitivity, the PAN/PVDF nanofiber-based QCM sensor was exposed to 7 different VOCs: chlorinated and non-chlorinated vapors. The sensitivity values for each vapor were calculated using QCM kinetic responses. The calculated values are presented in Table 6.

The best sensitivity values were obtained for the chlorinated vapors. BTX vapors showed the lowest sensitivities among all vapors tested. The sensitivity to xylene was approximately one-third of that to dichloromethane vapor.

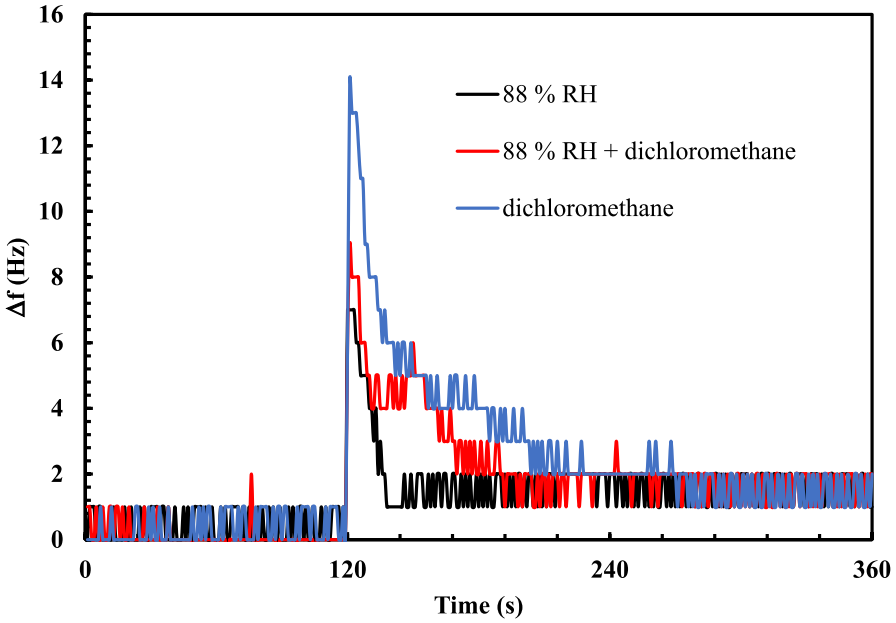

Fig. 13 The humidity effect response of the PAN/PVDF nanofiber-based QCM sensor

Conclusions

In this work, PAN/PVDF nanofibers were successfully fabricated by the electrospinning technique and utilized as an active layer in QCM-based vapor sensors. Morphological, structural, thermal, and mechanical characterizations confirmed the formation of uniform and stable nanofibers with improved thermal resistance and mechanical flexibility resulting from the synergistic interaction between PAN and PVDF. The adsorption studies revealed that the PAN/PVDF nanofiber-coated QCM sensor exhibited reproducible and sensitive responses to vapor molecules, demonstrating its potential for real-time VOC monitoring. The sensor performance metrics of the PAN/PVDF nanofiber-based QCM sensors were calculated for sensitivity (0.205–0.249 Hz ppm^{-1}), LOD (160.57–132.53 ppm), and LOQ (487.80–401.60 ppm), respectively. The sensor performance parameters, such as humidity effect, long-term stability, reversibility over many cycles, and selectivity parameters against DCM vapor, were studied. Results indicated that the sensor exhibited long-term stability and a reversible, selective response to DCM vapor. The humidity effect on the PAN/PVDF nanofiber-based QCM sensors could be negligible.

The pseudo-first-order and Elovich kinetic models effectively described the adsorption process, indicating that both physical and chemical adsorption mechanisms contributed to the overall interaction. These findings highlight the potential of PAN/PVDF hybrid nanofibers as high-performance sensing materials for advanced environmental and analytical applications. Future work may focus on optimizing

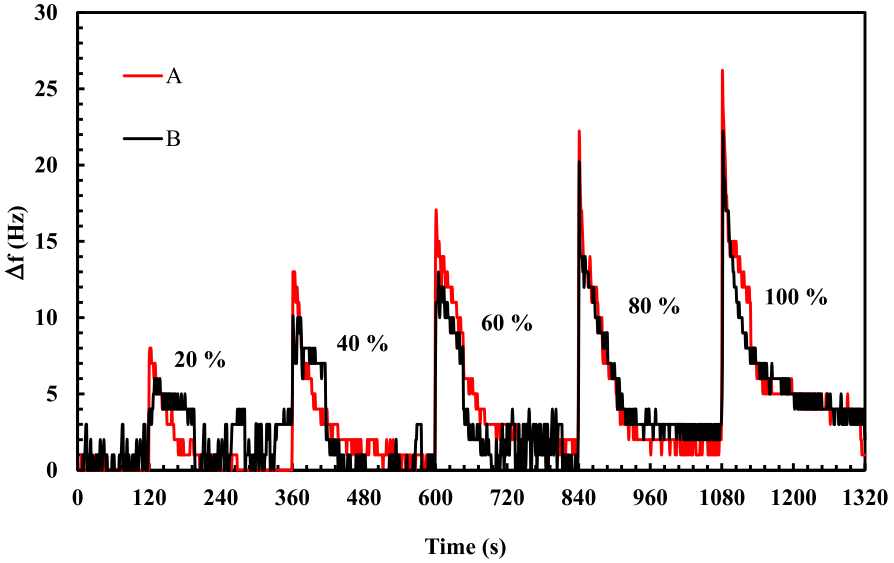

Fig. 14 Dichloromethane vapor exposure in increasing vapor amount (20%, 40%, 60%, 80%, and 100% saturated vapor). A is two years before, B is two years after

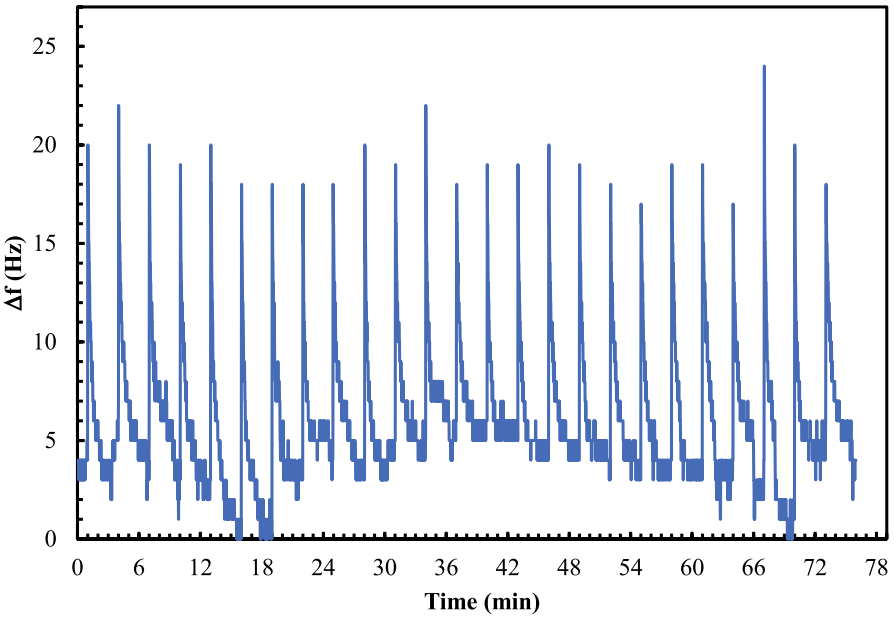

Fig. 15 Reversible interactions of the PAN/PVDF nanofiber-based QCM sensor over multiple cycles with DCM vapor

Table 6 The selectivity behavior toward chlorinated and non-chlorinated VOCs of the PAN/PVDF nanofiber-based QCM sensor

Vapor	Sensitivity (Hz/ppm)
Dichloromethane	0.0249
Chloroform	0.0245
Carbon tetrachloride	0.0234
Trichloroethylene	0.0205
Benzene	0.0183
Toluen	0.0102
Xylene	0.0082

fiber composition and morphology to further enhance selectivity and sensitivity toward specific target analytes.

Supplementary Information The online version contains supplementary material available at https://doi.org/10.1007/s11164-025-05897-7.

Author contributions Author contributions RC contributed to the supervision, investigation, formal analysis, conceptualization, methodology, data curation, investigation, writing-original draft, review, and editing. IC, AI and YA contributed to investigation, formal analysis, conceptualization, methodology, data curation, investigation, review, and editing.

Funding Open access funding provided by the Scientific and Technological Research Council of Türkiye (TÜBİTAK).

Data availability No datasets were generated or analysed during the current study.

Code availability Data will be made available on reasonable request.

Declarations

Conflict of interest The authors declare no confict of interest.

References

1. F. Han, T. Wang, Y. Chen, X. Ren, Z. Peng, X. Zheng, K. Wang, Y. Gao, Y. Cheng, G. Gao, Aligned triboelectric all-nanofiber generator as self-powered sensors for message cryptography. Compos. Part B Eng. **306**, 112835 (2025)
2. A.B. Yoruk, Y. Aykut, R. Eren, Y. Oz, Enhanced vibration detection with rGO-doped PAN/PVDF molecularly blended nanofibers: preparation and characterization of the nanofibrous flexible piezoelectric vibration sensing elements. Sens. Actuators A Phys. **393**, 116850 (2025)

3. Y. Sun, Y. Liu, Y. Zheng, Z. Li, J. Fan, L. Wang, X. Liu, J. Liu, W. Shou, Enhanced energy harvesting ability of ZnO/PAN hybrid piezoelectric nanogenerators. ACS Appl. Mater. Interfaces **12**, 54936–54945 (2020)
4. J. Zhang, K. Guo, J. Guo, M.A.A. Newton, T. Li, B. Xin, Unidirectional moisture-wicking PAN/BTO-PVDF/ZnO all fibrous bilayer breathable electronic skin for health sensing. Polymer **316**, 127815 (2025)
5. A. Khadka, E. Samuel, B. Joshi, A. Aldalbahi, G. Periyasami, H.S. Lee, S.S. Yoon, Integrating PVDF-based piezoelectric nanogenerators with highly conductive carbon nanofibers for energy-harvesting applications. Nano Energy **139**, 110991 (2025)
6. A. Rianjanu, F. Fauzi, K. Triyana, H.S. Wasisto, Electrospun nanofibers for quartz crystal microbalance gas sensors: a review. ACS Appl. Nano Mater. **4**(10), 9957–9975 (2021)
7. A.I. Yardimci, N. Yagmurcukardes, M. Yagmurcukardes, I. Capan, M. Erdogan, R. Capan, O. Tarhan, Y. Acikbas, Electrospun polyacrylonitrile (PAN) nanofiber: preparation, experimental characterization, organic vapor sensing ability and theoretical simulations of binding energies. Appl. Phys. A **128**, 173 (2022)
8. N. Yagmurcukardes, A.I. Yardimci, M. Yagmurcukardes, I. Capan, M. Erdogan, R. Capan, Y. Acikbas, Electrospun polyacrylonitrile (PAN)/polypyrrole (PPy) nanofber–coated quartz crystal microbalance for sensing volatile organic compounds. J. Mater. Sci. Mater. Electron. **34**, 1869 (2023)
9. A.I. Yardimci, K. Buyukkabasakal, I. Capan, R. Capan, S. Bitar, Y. Acikbas, Electrospun polyacrylonitrile/polyvinylidene fluoride nanofiber-coated QCM: preparation, characterization, gas sensing properties, and data validation via artificial neural networks. ChemistrySelect **10**, e202405144 (2025)
10. M. Febrina, A. Rianjanu, A. Rajak, R.R. Mukti, M. Djamal, Electrospun polyacrylonitrile nanofibers mixed with citric acid as a quartz crystal microbalance ammonia vapor sensor. ChemistrySelect **7**, e202103615 (2022)
11. A. Rianjanu, K. Triyana, N. Nurbaiti, S.A. Hasanah, A. Kusumaatmaja, R. Roto, An enhanced safrole sensing performance of a polyacrylonitrile nanofiber-based-QCM sensor by overlaying with chitosan. Sains Malaysiana **48**(9), 2041–2049 (2019)
12. Y.M. Rohman, R. Sukowati, A. Priyanto, D.A. Hapidin, D. Edikresnha, K. Khairurrijal, Quartz crystal microbalance coated with polyacrylonitrile/nickel nanofibers for high-performance methanol gas detection. ACS Omega **8**, 13342–13351 (2023)
13. R. Capan, I. Capan, M. Bayrakci, Sensor parameters and adsorption behaviour of rhodamine-based polyacrylonitrile (PAN) nanofiber against dichloromethane vapour. Microchem. J. **207**, 111806 (2024)
14. R. Capan, I. Capan, M. Bayrakci, Quartz crystal microbalance modified with rhodamine-polyacrylonitrile nanofibers for acetone vapor sensing. Mater. Sci. Eng. B Solid-State Mater. Adv. Technol. **322**, 118581 (2025)
15. R. Capan, I. Capan, M. Bayrakcı, Rhodamine-based electrospun polyacrylonitrile (PAN) nanofiber sensor for the detection of chlorinated hydrocarbon vapors. ACS Appl. Polym. Mater. **6**(13), 7500–7511 (2024)
16. R. Sukowati, Y.M. Rohman, B.H. Agung, D.A. Hapidin, H. Damayanti, K. Khairurrijal, An investigation of the influence of nanofibers morphology on the performance of QCM-based ethanol vapor sensor utilizing polyvinylpyrrolidone nanofibers active layer. Sens. Actuators B Chem. **386**, 133708 (2023)
17. F. Temel, One novel calix[4]arene based QCM sensor for sensitive, selective and high performance-sensing of formaldehyde at room temperature. Talanta **211**, 120725 (2020)
18. R. Capan, I. Capan, F. Davis, A new approach for the adsorption kinetics using surface plasmon resonance results. Sens. Actuators B Chem. **394**, 134463 (2023)
19. S. Wang, L. Huang, Y. Zhang, L. Li, X. Lu, A mini-review on the modeling of volatile organic compound adsorption in activated carbons: equilibrium, dynamics, and heat effects. Chin. J. Chem. Eng. **31**, 153–163 (2021)
20. B. Liu, H. Luo, H. Rong, X. Zeng, K. Wu, Z. Chen, H. Lu, D. Xu, Temperature-induced adsorption and desorption of phosphate on poly(acrylic acid-co-N-[3-(dimethylamino)propyl]acrylamide) hydrogels in aqueous solutions. Desalination Water Treat. **160**, 260–267 (2019)
21. M. Pourtalari, A.H. Hassani, E. Moniri, A.H. Javid, and H.A. Panahi, Effective defluoridation of industrial wastewater using free radical graft polymerization onto the mesoporous alumina: experimental and response surface methodology modeling, J. Ind. Eng. Chem. (in press 2025)

22. L. Largitte, R. Pasquier, A review of the kinetics adsorption models and their application to the adsorption of lead by an activated carbon. Chem. Eng. Res. Des. **109**, 495–504 (2016)
23. F. Yalcinkaya, B. Yalcinkaya, A. Pazourek, J. Mullerova, M. Stuchlik, J. Maryska, Surface modification of electrospun PVDF/PAN nanofibrous layers by low vacuum plasma treatment. Int. J. Polym. Sci. **4671658**, 1–9 (2016)
24. S. Keikhaei, Z. Mohammadalizadeh, S. Karbasi, A. Salimi, Evaluation of the effects of β-tricalcium phosphate on physical, mechanical and biological properties of poly (3-hydroxybutyrate)/chitosan electrospun scaffold for cartilage tissue engineering applications. Mater. Technol. **34**(10), 615–625 (2019)
25. G. Sauerbrey, Verwendung von schwingquarzen zur wagungdünner schichten und zur mikrowagung. Z. Phys. **155**, 206–222 (1959)
26. K. Srivastava, P. Sakthivel, Quartz-crystal microbalance study for characterizing atomic oxygen in plasma ash tools. J. Vacuum Sci. Tech. A **19**(1), 97–100 (2001)
27. M. Kumar, M.K. Singh, G. Arora, S.K. Palaniappan, V. Ayyappan, G.P. Muthukutti, K. Vijayanath, S.M. Rangappa, S. Siengchin, A comprehensive review on next-gen electrospun nanofibers for multidirectional applications from energy storage to precise medicine, Macromol. Res. **33**, 1613-1648 (2025)
28. S. Yavari, M. Sembay, Y. Bushanov, Z. Bakenov, M. Shafiee, G. Kalimuldina, Recycling Recycling Polyvinyl Chloride (PVC) Pipe Wastes into PVC/ZnO Nanofiber-Based Triboelectric Nanogenerators. Energy Environ. Mat. **8**, e12884 (2025)
29. L. Katriani, R. Aflaha, A.H. As'ari, P. Nurwantoro, R. Roto, K. Triyana, Nanofiber-coated quartz crystal microbalance with chitosan overlay for highly sensitive room temperature ammonia gas sensor. Microchem. J. **206**, 111532 (2024)
30. A. Rianjanu, M.A. Rayhan, M. Aulya, R. Aflaha, K. Triyana, T. Taher, H.S. Wasisto, Early spoilage detection of cultured pacific white shrimp using quartz crystal microbalance gas sensors. ChemistrySelect **9**, e202304694 (2024)
31. R.A.Q.B. Al-Marjeh, Y. Atassi, N. Mohammad, Y. Badour, Adsorption of methyl orange onto electrospun nanofiber membranes of PLLA coated with pTSA-PANI. Environ. Sci. Pollut. Res. **26**, 37282–37295 (2019)
32. T. Wang, Y. Chen, W. Dong, Y. Liu, L. Shi, R. Chen, T. Pan, Fractal characteristics of porosity of electrospun nanofiber membranes. Math. Probl. Eng. **1**, 2503154 (2020)
33. R. Murphy, A. Turcott, L. Banuelos, E. Dowey, B. Goodwin, K.O.H. Cardinal, Simpoly: a Matlab-based image analysis tool to measure electrospun polymer scaffold fiber diameter. Tissue Eng. Part C Methods **26**(12), 628–636 (2020)
34. L. Chen, L. Bromberg, H. Schreuder-Gibson, J. Walker, T.A. Hatton, G.C. Rutledge, Chemical protection fabrics via surface oximation of electrospun PAN mats. J. Mater. Chem. **19**(16), 2432–2438 (2009)
35. A. Biswas, K. Henkel, D. Schmeißer, D. Mandal, Comparison of the thermal stability of the α, β and γ phases in poly (vinylidene fluoride) based on in situ thermal Fourier transform infrared spectroscopy. Phase Trans. **90**(12), 1205–1213 (2017)
36. C. Merlini, GMd.O. Barra, S.DAd.S. Ramôa, G. Contri, Rd.S. Almeida, MAd.' Ávila, B.G. Soares, Electrically conductive polyaniline-coated electrospun poly (vinylidene fluoride) mats. Front. Mater. **2**, 14 (2015)
37. A.I. Gopalan, P. Santhosh, K.M. Manesh, J.H. Nho, S.H. Kim, C.-G. Hwang, K.-P. Lee, Development of electrospun PVdF–PAN membrane-based polymer electrolytes for lithium batteries. J. Membr. Sci. **325**, 683–690 (2008)
38. R.M. Elkhaldi, S. Guclu, I. Koyuncu, Enhancement of mechanical and physical properties of electrospun PAN nanofiber membranes using PVDF particles. Desalination Water Treat. **57**, 26003–26013 (2016)
39. C. Luo, J. Wang, P. Jia, Y. Liu, J. An, B. Cao, K. Pan, Hierarchically structured polyacrylonitrile nanofiber mat as highly efficient lead adsorbent for water treatment. Chem. Eng. J. **262**, 775–784 (2015)
40. A.J. de Jesus Silva, M.M. Contreras, C.R. Nascimento, M.F. da Costa, Kinetics of thermal degradation and lifetime study of poly (vinylidene fluoride)(PVDF) subjected to bioethanol fuel accelerated aging. Heliyon **6**(7), e04573 (2020)
41. A.M. Abd El-Aziz, M. Afifi, Influence the β-PVDF phase on structural and elastic properties of PVDF/PLZT composites. Mater. Sci. Eng. B Solid-State Mater. Adv. Technol. **301**, 117152 (2024)

42. L. Xu, X. Hu, Y.T. Lim, V.S. Subramanian, Organic vapor adsorption behavior of poly(3-butoxythiophene) LB films on quartz crystal microbalance. Thin Solid Films **417**, 90–94 (2002)
43. I. Capan, M. Erdogan, G.A. Stanciu, S.G. Stanciu, R. Hristu, M. Göktepe, The interaction between the gas sensing and surface morphology properties of LB thin f ilms of porphyrins in terms of the adsorption kinetics. Mater. Chem. Phys. **136**, 1130–1136 (2012)
44. A.N. Sahin, A. Altındal, Z.G. Ozdemir, Acetone and isopropyl alcohol vapor sensing properties of NiO films under varying bias voltages at room temperature. Phys. Status Solidi A Appl. Mater. Sci. **222**(11), 2400891 (2025)
45. N.L.L.Hekiem, A.A. Ralib, M.A.M. Hatta, F.B. Ahmad, R. Rahim, and N.F. Zabah; Performance analysis of VOCs detection using polyisobutylene and chitosan overlayed on QCM sensor, IEEE regional symposium on micro and nanoelectronics (RSM) (2021)
46. V. Yılmaz, N. Can, A. Altındal, Adsorption of VOC vapors on ZnPc: sensing and kinetic studies. Environ. Sci. Pollut. Res. **31**, 65302–65314 (2024)
47. G.S.K.D. Vijayalakshmi, N. Puvvada, Recent advances in chemically engineered nanostructures impact on ischemic stroke treatment. ACS Omega **8**(48), 45188–45207 (2023)
48. A. Rianjanu, R. Roto, T. Julian, S.N. Hidayat, A. Kusumaatmaja, E.A. Suyono, K. Triyana, Polyacrylonitrile nanofiber-based quartz crystal microbalance for sensitive detection of safrole. Sensors **18**(4), 1150 (2018)
49. K. Triyana, A. Rianjanu, D.B. Nugroho, A.H. Asari, A. Kusumaatmaja, R. Roto, R. Suryana, H.S. Wasisto, A highly sensitive safrole sensor based on polyvinyl acetate (PVAc) nanofiber-coated QCM. Sci. Rep. **9**, 15407 (2019)
50. A. Rianjanu, K. Triyana, D.B. Nugroho, A. Kusumaatmaja, R. Roto, Electrospun polyvinyl acetate nanofiber modified quartz crystal microbalance for detection of primary alcohol vapor. Sens. Actuators A **301**, 111742 (2020)
51. X. Wu, X. Wang, Y. Hu, H. Chen, X. Liu, X. Dang, Adsorption mechanism study of multinuclear metal coordination cluster Zn5 for anionic dyes congo red and methyl orange: experiment and molecular simulation. Appl. Surf. Sci. **586**, 152745 (2022)

Authors and Affiliations

Rifat Capan[1] · Atike Ince Yardimci[2] · Inci Capan[1] · Yaser Acikbas[3]

✉ Rifat Capan
rcapan@balikesir.edu.tr

Atike Ince Yardimci
atike.yardimci@usak.edu.tr

Inci Capan
ibasaran@balikesir.edu.tr

Yaser Acikbas
yaser.acikbas@usak.edu.tr

[1] Physics Department, Science & Literature Faculty, Balikesir University, 10145 Balikesir, Turkey

[2] Technology Transfer Office, Usak University, 64200 Usak, Turkey

[3] Electrical and Electronics Engineering Department, Engineering and Natural Sciences Faculty, Usak University, 64200 Usak, Turkey